NANO LETTERS

2007
Vol. 7, No. 12
3681−3685

Correlating Luminescence from Individual ZnO Nanostructures with Electronic Transport Characteristics

Young Mu Oh,[†] Kyung Moon Lee,[†] Kyung Ho Park,[‡] Yongsun Kim,[†] Y. H. Ahn,[†] Ji-Yong Park,*[,†] and Soonil Lee[†]

Division of Energy Systems Research, Ajou University, Suwon, 443-749, Korea, and Korea Advanced Nano Fab Center, Suwon, 443-766, Korea

Received August 7, 2007; Revised Manuscript Received October 5, 2007

ABSTRACT

Cathodoluminescence (CL) emissions from individual ZnO nanostructures with diameters of 30–100 nm are investigated to correlate their optical and electrical properties. Two types of ZnO nanostructures with high and low charge carrier densities are identified from electronic transport measurements and concomitant CL characterizations. The results demonstrate that local luminescence characterizations can provide information about inhomogeneities in electrical and optical properties among ZnO nanostructures.

ZnO is a promising material for various optical and electrical applications and have been foci of active researches.[1,2] As a direct band gap semiconductor ($E_g = 3.3$ eV) with a high exciton binding energy of 60meV, ZnO has potentials for various optical applications such as light-emitting diodes[3] and lasers.[4] On the other hand, ZnO has also attracted interests due to possible applications as an electronic material. Devices such as field effect transistors,[5] transparent electrodes,[6] and gas sensors[7] based on ZnO have been demonstrated.

In recent years, ZnO-based nanostructures such as nanowires (NWs), nanoneedles, nanorods, and tri- or tetrapods (TPs) have attracted interest because they can be used as building blocks for future optical, electrical, or optoelectronic devices with their small sizes, large surface-to-volume ratio, good crystallinity, and so on.[8,9] Photoluminescence (PL) has been an invaluable tool in investigating optical characteristics of ZnO-based nanostructures[10] and in accessing their qualities. When excited by light with energies larger than band gap, PL from ZnO-based nanostructures mainly consists of luminescence at ∼380 nm due to excitonic recombinations near band edge[11] and luminescence at visible ranges such as green luminescence at ∼510 nm due to deep defect states inside band gap.[10−18] Strong luminescence at ∼380 nm compared to visible luminescence is often regarded as an indication of defect-free, crystalline ZnO structures.[19] Although PL measurements from individual semiconducting NWs are possible,[20] spatial resolutions are limited due to the diffraction limit and poor signal-to-noise ratio. In most cases, PL is taken from ensembles of nanostructures, which makes it difficult to investigate local or individual characteristics of nanostructures under illuminations. In this aspect, cathodoluminescence (CL) measurements, which record luminescence after creating electron−hole pairs by high-energy electron bombardment, can be complementary to PL measurements[21,22] and provide more information with its high spatial resolution, especially for nanostructures.[23−27] Luminescence that originates from defects such as green luminescence can be related to the electronic characteristics of nanostructures, because defects are also responsible for the electrical properties of the materials.[2] Although, there have been some reports of correlations between luminescence and electronic properties in ZnO,[28,29] little is known about ZnO nanostructures.

In this letter, we report the use of CL as a local luminescence characterization tool of ZnO nanostructures. CL images and spectra of individual ZnO nanostructures are obtained, and their correlations to the electronic transport characteristics of the same nanostructures are investigated. It was found that two distinct types of ZnO nanostructures exist as confirmed by CL and transport measurements.

ZnO nanostructures were synthesized using thermal chemical vapor deposition method.[19,30] An equal amount of ZnO powder and graphite powder are used as source materials. The source materials are heated to 1000 °C in the furnace and typically kept at that temperature for 2 h under a constant flow of N_2 gas. White powders collected from cold (<200 °C) area of the quartz tube contain ZnO nanostructures such as NWs and TPs with diameters between 30 and 100 nm.

* Corresponding author. E-mail: jiyong@ajou.ac.kr.
[†] Ajou University.
[‡] Korea Advanced Nano Fab Center.

10.1021/nl071959o CCC: $37.00
Published on Web 11/14/2007

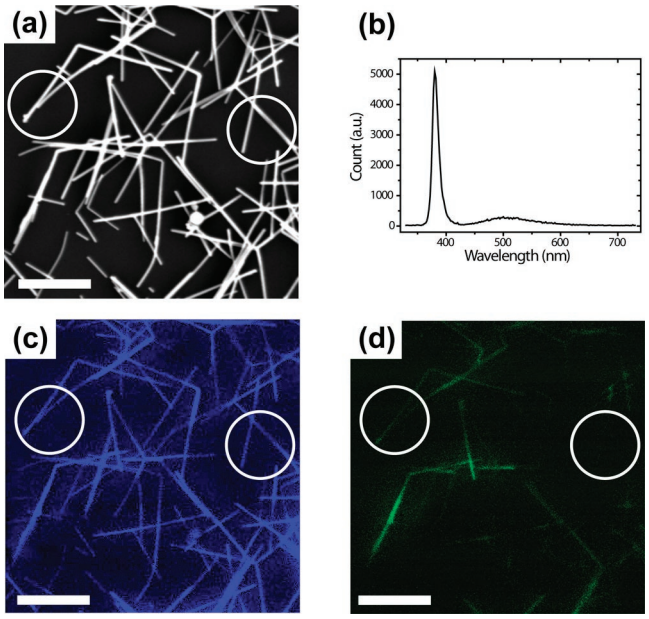

Figure 1. (a) An SEM image of ZnO nanostructures on a Si substrate. (b) A CL emission spectrum obtained from the same area as in panel a. (c) A monochromatic CL image of panel a at 380 nm. (d) A monochromatic CL image of panel a at 510 nm. Scale bars in all images are 1 μm.

White powders containing ZnO nanostructures are dispersed in methanol with ultrasonic agitation and deposited onto highly doped ($<0.005\ \Omega\cdot$cm) Si substrates with 200 nm of SiO_2 layer. Source and drain electrodes with 2−6 μm gaps are formed on the ZnO nanostructures by patterning with photolithography, metal deposition with e-beam evaporations, and subsequent lift-off processes. Ti (70 nm thick) with Au-capping layer (10 nm thick) is used as metal electrodes for all the ZnO devices used for the measurements. Topographic images of synthesized ZnO nanostructures and fabricated ZnO devices are investigated using an atomic force microscope (AFM) and a scanning electron microscope (SEM). CL measurements are performed at room temperature with a Gatan MonoCL3+ system equipped with a high-sensitivity photo multiplier tube (PMT) (thermoelectrically cooled to −20 °C) attached to an SEM (S-4300SE from Hitachi). Acceleration voltage of 10 kV is used for all the CL measurements presented in this paper. 3-Terminal electronic transport characteristics are investigated using a semiconductor parameter analyzer (4156C from Agilent).

ZnO nanostructures synthesized are mostly NWs or TPs in the diameter range between 30 and 100 nm as confirmed both using AFM and SEM measurements. A representative SEM image of ZnO nanostructures is shown in Figure 1a. The synthesized ZnO nanostructures are dispersed and dropped on a Si substrate for measurements. Their luminescence spectra are investigated by both PL and CL, which show similar peak positions. Luminescence spectra from these ZnO nanostructures typically show a strong peak at ∼380 nm and a weak peak at ∼510 nm.

A CL spectrum from same ZnO nanostructures in Figure 1a is shown in Figure 1b. The stronger luminescence at 380 nm is due to the band gap of ZnO, and the weak one at ∼510 nm is due to defect states as mentioned in the introduction. There are two ways to get CL images. One is panchromatic CL images in which the image is formed by plotting integrated luminescence of the whole wavelength range of the PMT detector (160∼930 nm) at each point of electron beam irradiation. The other is monochromatic CL images in which only luminescence at the particular wavelength is plotted by adjusting the spectrometer. Monochromatic images typically show poorer signal-to-noise ratio than panchromatic ones but contain spectroscopic information. All the CL images presented in this paper are monochromatic ones. Monochromatic CL images of the same area as seen in Figure 1a are taken at 380 and 510 nm as shown in Figure 1, panels c and d, respectively. In comparison to Figure 1a, it can be seen that almost all the ZnO nanostructures give strong emission at 380 nm as shown in Figure 1c. ZnO NWs as close as ∼50 nm are distinguishable in Figure 1c, demonstrating high resolution of the CL imaging. In this case, the nanostructures themselves set the spatial resolution in CL images because their sizes are smaller than the electron penetration depth unlike the bulk case. Differences in emission intensities are believed mostly due to the differences in the sizes of the nanostructures, which result in different generation volumes for CL. However, much stronger inhomogeneities, which cannot be accounted for only by differences in their sizes, are found in the monochromatic CL image taken at 510 nm as shown in Figure 1d. This image shows that not all the ZnO nanostructures give CL emission at 510 nm, but rather only a small number of ZnO nanostructures participate in the luminescence at 510 nm. All the ZnO NWs with similar diameters as enclosed by circles in Figure 1a,c,d give similar CL emission at 380 nm, but only NWs inside the left circle show emissions at 510 nm. These images demonstrate that a luminescence spectrum such as Figure 1b sometimes cannot represent the optical characteristics of all the nanostructures inside the probing area, due to inhomogeneities among the nanostructures. Only with the high-resolution spatial-imaging capability of CL in SEM was it possible to identify the inhomogeneities in the green emission among ZnO nanostructures, which implies different defect intensities among ZnO nanostructures, although they were synthesized and collected in the same batch and at the same location.

Current−voltage ($I-V$) characteristics of these ZnO nanostructures are investigated after source and drain electrodes are fabricated on the dispersed ZnO nanostructures. Highly doped Si substrates with SiO_2 layers are used as gate electrodes. By taking current (I_{DS}) versus gate voltage (V_G) traces of individual ZnO nanostructures, ZnO nanostructures could be classified into two types based on their responses to the gate electric fields. There is one type of ZnO nanostructures that shows typical n-type semiconducting behaviors with large on−off ratios ($>10^6$) (Type I). The other type of ZnO nanostructures exists and shows very weak n-type gate dependence even for the gate voltage range of −80 to 80 V so that they can be classified as metallic (Type II). After characterizing transport properties of ZnO devices, CL images and spectra are also obtained on the same devices. Results from two ZnO devices fabricated with ZnO TPs with

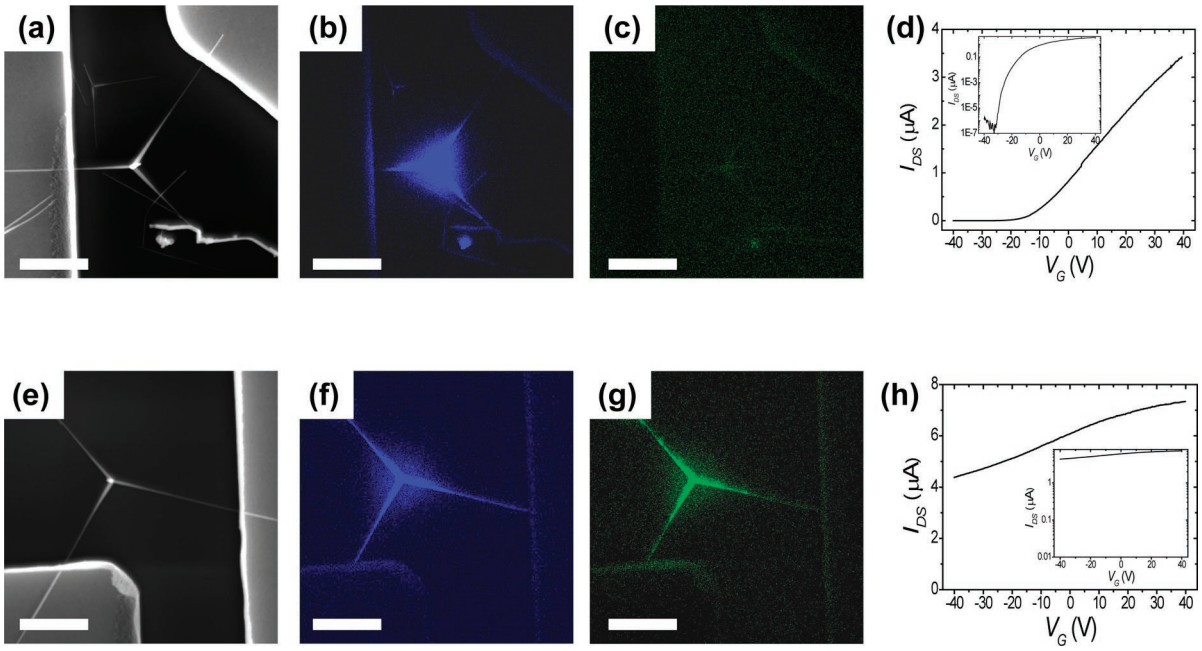

Figure 2. (a) An SEM image, (b) a monochromatic CL image at 380 nm, (c) a monochromatic CL image at 510 nm, and (d) an I_{DS} vs V_G curve of a type I device with a ZnO TP. (e) An SEM image, (f) a monochromatic CL image at 380 nm, (g) a monochromatic CL image at 510 nm, and (h) an I_{DS} vs V_G curve of a type II device with a ZnO TP. Insets in panels d and h are I_{DS} vs V_G curves with log scales in the *y*-axis. Scale bars in all images are 2 μm.

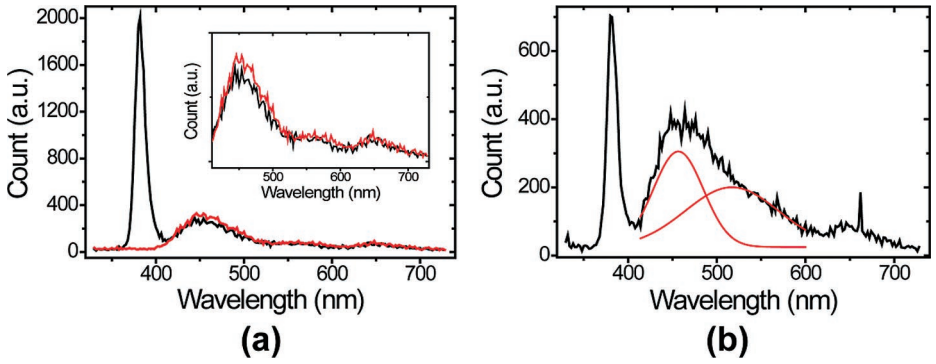

Figure 3. (a) CL emission spectra from the type I device in Figure 2a−d (black) and from a nearby area without ZnO nanostructures (red). Both curves are almost identical except for the peak at 380 nm. Inset is a close-up view of the spectrum between 420 nm and 730 nm. (b) A CL emission spectrum from the type II device in Figure 2e−h (black). The asymmetric peak at ∼480 nm can be fitted by two peaks (red), centered ∼460 nm and ∼510 nm, respectively.

similar sizes but different transport characteristics are shown in Figure 2. for comparison (These two sets of data are chosen as representative ones due to their similar shapes and sizes. See Supporting Information for additional data for other types of ZnO nanostructure cases including NWs). *I*−*V* transport characteristics of TPs at room temperature are found to be similar to those of NWs with similar diameters in our measurement. The device shown in Figure 2a−d is type I with an on−off ratio of $>10^6$ (inset of Figure 2d), while another device in Figure 2e−h is type II with only a factor of 2 current changes for the gate voltage range between −40 and 40V. Although both show quite strong luminescence at 380 nm as in Figure 2b,f, monochromatic images at 510 nm show big differences as shown in Figure 2c,g. While the type II device shows quite a big CL signal at 510 nm (Figure 2g), it is absent or below detection limit in the type I device (Figure 2c). Only a faint signal at the junction area is visible in Figure 2c, while type II device shows CL signal at 510 nm along the whole length of the nanostructures as in Figure 2g. A total of 11 ZnO devices made of ZnO NWs and TPs (6 type I and 5 type II) were examined in the same way, and all the type II devices exhibit green luminescence while all the type I devices show little or below detection limit green luminescence.

To clarify the differences, CL spectra for both devices were obtained at the same area as shown in Figure 2a,e, and they are plotted in Figure 3a,b, respectively. The CL spectrum from the type I device, imaged in Figure 2a−c, displays a strong peak at 380 nm, smaller peaks centered around 460 nm, and longer wavelengths as shown in Figure 3a. The peak at 460 nm is originated not from ZnO nanostructures but from the SiO_2 layer. SiO_2 is known to give luminescence at this peak, associated with E′ center defects in the bulk.[31] We also took a CL spectrum from an area about 5 μm away

from one in Figure 2a, containing no ZnO but with a similar area of SiO_2 and metal electrodes. It is also plotted in Figure 3a without normalization. Both spectra in Figure 3a are almost identical except the peak at 380 nm, which confirms that the peaks at 460 nm and longer wavelengths originate from the SiO_2 layer. From this, we can see that the ZnO TP shown in Figure 2a has negligible green emission, compared to the near band edge emission at 380 nm, which is consistent with monochromatic CL images in Figure 2b,c. We also took a CL spectrum from the type II device shown in Figure 2e, which is plotted in Figure 3b. This spectrum again shows a dominant peak at 380 nm, but it also shows a rather strong and asymmetric peak at ~480 nm. This peak can be nicely fit by two peaks at 460 and 510 nm, respectively, as shown in Figure 3b. This suggests that the visible CL spectrum from the type II device originates from both SiO_2 and defects, which have a strong emission at ~510 nm, resulting in the green emission CL image in Figure 2g. Both monochromatic CL images (Figure 2c,g) and spectrum (Figure 3a,b) point to the existence of a green emission in type II devices, while almost no or negligible emission from type I devices.

Near metallic behaviors in type II devices indicate larger free electron densities compared to type I devices. The charge densities, n_e, at different gate voltages, V_G, can be estimated as $en_e = C_G|V_G - V_{TH}|$. In this formula, V_{TH} is the threshold voltage and C_G is the gate capacitance, which can be estimated as $C_G \sim 2\pi\epsilon\epsilon_0 L/\ln(2h/r)$, where L is the channel length, h is the thickness of gate oxide, and r is the radius of the ZnO nanostructures. In the type II device in Figure 2, the threshold voltages could not be reached even down to −80 V so that only the lower limit on the charge density can be estimated from the same formula. We can see that there is at least an order of magnitude difference in charge densities at $V_G = 0$ between these two devices. The estimated mobilities of electrons from the slope of linear region in Figure 2d,h indicate that it is lower for the type II device due to the existence of more defects that act as scattering centers in the nanostructures. Therefore, we found that ZnO nanostructures with high carrier densities (high n-type doping) have stronger luminescence at ~510 nm, compared to ones with smaller carrier densities.

There are still controversies about the origin of the green luminescence often observed in ZnO materials.[10] It is often attributed to single-ionized oxygen vacancies,[12,13,28] but other assignments such as interstitial Zn,[32] defect complexes,[14] and impurities such as Cu[33] are suggested in the literatures. Because they have to originate from deep trap states inside the band gap, they are not directly related to the defects that act as shallow donors for ZnO and are responsible for the n-type behaviors. Surface or bulk oxygen vacancies are often cited as the origin of n-type conduction in ZnO, which has been questioned in recent years.[2] Oxygen vacancies, zinc interstitials, or hydrogen are thought to be responsible for the n-type conduction. Although the green luminescence is not directly related to those shallow donors, the density of defects giving green luminescence can be proportional to that of shallow donors if they have similar origins such as different charging states of oxygen vacancies. This would explain the relationship between high carrier density and green luminescence observed in this experiment. There is also a possibility that the green luminescence and n-type doping have different origins. Then, our result can be related to the surface depletion of electrons in ZnO nanostructures. Metal oxide materials like ZnO are well known for their gas-sensing capabilities, and it is due to the formation of depletion regions near the surface upon gas adsorption such as oxygen.[8] This results in surface depletion of electrons, which controls conduction in ZnO. Because the depletion width is inversely proportional to the square of the charge density in the bulk, we can expect that the type II device with larger carrier density will have smaller depletion width. In the bulk, the deep level states lie below Fermi level so that they are filled and the green luminescence can be expected by recombination of these electrons with photo-excited holes. But near the surface area inside the depletion width, parts of the deep level states can lie above the Fermi level due to band bending so that they are unoccupied and may not give green luminescence. In this way, we can expect that more generation volumes for green luminescence are available for type II devices. This effect can be significant in the nanostructures because the Debye length can be comparable to the size of the nanostructures. These two effects, the density of defects and/or different depletion layer widths, are believed to be responsible for the correlations between green emissions and charge carrier densities in ZnO nanostructures. Current results with additional data shown in the Supporting Information do not imply any correlation between luminescence characteristics with the size or kind of nanostructures. The apparent correlation we found is one between the presence of green luminescence and charge carrier densities as explained before. To fully understand the origin of the correlation between luminescence and transport characteristics, more systematic investigation of samples are necessary by comparing differences among samples with similar kinds and sizes or carrier densities. The inhomogeneities observed among ZnO nanostructures even grown and collected together can be attributed to fluctuations during growth and formation of the nanostructures, such as different oxygen consumptions during growth processes. Investigation of inhomogeneities among ZnO nanostructures grown in different methods can shed some light on the fundamental growth mechanisms and their improvements.

In conclusion, we have shown that local luminescence measurements by CL can give information about optical characteristics of nanostructures with high spatial resolution. Inhomogeneties in optical and electrical properties among ZnO-based nanostructures are observed. Two types of ZnO nanostructures with high- and low-carrier densities are identified both by CL and electronic transport measurements. These results indicate that correlating various optical or electrical properties of ZnO nanostructures by measuring luminescence spectra from collections of ZnO nanostructures can be misleading and should be taken at least with caution in view of possible inhomogeneities among nanostructures as demonstrated in this paper. Local luminescence measure-

ments with CL demonstrated in this paper can be extended to other nanostructures with direct band gaps as well.

Acknowledgment. This work was supported by the Korea Research Foundation Grant funded by the Korean Government (MOEHRD) (KRF-2005-041-C00168) and by the Ministry of Science and Technology through the Nanoscopia Center of Excellence at Ajou University.

Supporting Information Available: More type I devices are shown in Figures S1 and S3, and more type II devices are shown in Figures S2 and S4. This material is available free of charge via the Internet at http://pubs.acs.org.

References

(1) Klingshirn, C. *ChemPhysChem* **2007**, *8*, 782−803.
(2) Schmidt-Mende, L.; MacManus-Driscoll, J. L. *Mater. Today* **2007**, *10*, 40−48.
(3) Tsukazaki, A.; Ohtomo, A.; Onuma, T.; Ohtani, M.; Makino, T.; Sumiya, M.; Ohtani, K.; Chichibu, S. F.; Fuke, S.; Segawa, Y.; Ohno, H.; Koinuma, H.; Kawasaki, M. *Nat. Mater.* **2005**, *4*, 42−46.
(4) Bagnall, D. M.; Chen, Y. F.; Zhu, Z.; Yao, T.; Koyama, S.; Shen, M. Y.; Goto, T. *Appl. Phys. Lett.* **1997**, *70*, 2230−2232.
(5) Fortunato, E. M. C.; Barquinha, P. M. C.; Pimentel, A.; Goncalves, A. M. F.; Marques, A. J. S.; Pereira, L. M. N.; Martins, R. F. P. *Adv. Mater.* **2005**, *17*, 590−594.
(6) Fortunato, E.; Ginley, D.; Hosono, H.; Paine, D. C. *MRS Bull.* **2007**, *32*, 242−247.
(7) Moseley, P. T. *Sens. Actuators, B* **1992**, *6*, 149−156.
(8) Kolmakov, A.; Moskovits, M. *Annu. Rev. Mater. Res.* **2004**, *34*, 151−180.
(9) Wang, Z. L. *J. Phys.: Condens. Matter* **2004**, *16*, R829−R858.
(10) Djurišić, A. B.; Leung, Y. H. *Small* **2006**, *2*, 944−961.
(11) Meyer, B. K.; Alves, H.; Hofmann, D. M.; Kriegseis, W.; Forster, D.; Bertram, F.; Christen, J.; Hoffmann, A.; Strassburg, M.; Dworzak, M.; Haboeck, U.; Rodina, A. V. *Phys. Status Solidi B* **2004**, *241*, 231−260.
(12) Vanheusden, K.; Warren, W. L.; Seager, C. H.; Tallant, D. R.; Voigt, J. A.; Gnade, B. E. *J. Appl. Phys.* **1996**, *79*, 7983−7990.
(13) van Dijken, A.; Meulenkamp, E. A.; Vanmaekelbergh, D.; Meijerink, A. *J. Lumin.* **2000**, *87−89*, 454−456.
(14) Djurišić, A. B.; Choy, W. C. H.; Roy, V. A. L.; Leung, Y. H.; Kwong, C. Y.; Cheah, K. W.; Rao, T. K. G.; Chan, W. K.; Lui, H. T.; Surya, C. *Adv. Funct. Mater.* **2004**, *14*, 856−864.
(15) Hsu, N. E.; Hung, W. K.; Chen, Y. F. *J. Appl. Phys.* **2004**, *96*, 4671−4673.
(16) Ong, H. C.; Du, G. T. *J. Cryst. Growth* **2004**, *265*, 471−475.
(17) Bertram, F.; Christen, J. *Acta Phys. Pol., A* **2006**, *110*, 103−110.
(18) Borseth, T. M.; Svensson, B. G.; Kuznetsov, A. Y.; Klason, P.; Zhao, Q. X.; Willander, M. *Appl. Phys. Lett.* **2006**, *89*, 262112.
(19) Huang, M. H.; Wu, Y.; Feick, H.; Tran, N.; Weber, E.; Yang, P. *Adv. Mater.* **2001**, *13*, 113−116.
(20) Wang, J.; Gudiksen, M. S.; Duan, X.; Cui, Y.; Lieber, C. M. *Science* **2001**, *293*, 1455−1457.
(21) Phillips, M. R. *Microchim. Acta* **2006**, *155*, 51−58.
(22) Petrov, V. I. *Phys.-Usp.* **1996**, *39*, 807−816.
(23) Fan, H. J.; Scholz, R.; Zacharias, M.; Gosele, U.; Bertram, F.; Forster, D.; Christen, J. *Appl. Phys. Lett.* **2005**, *86*, 023113.
(24) Chen, C. W.; Chen, K. H.; Shen, C. H.; Ganguly, A.; Chen, L. C.; Wu, J. J.; Wen, H. I.; Pong, W. F. *Appl. Phys. Lett.* **2006**, *88*, 241905.
(25) Piechal, B.; Yoo, J.; Elshaer, A.; Mofor, A. C.; Yi, G. C.; Bakin, A.; Waag, A.; Donatini, F.; Dang, L. S. *Phys. Status Solidi B* **2007**, *244*, 1458−1461.
(26) Chang, Y. C.; Chen, L. J. *J. Phys. Chem. C* **2007**, *111*, 1268−1272.
(27) Wang, R. C.; Liu, C. P.; Huang, J. L.; Chen, S. J. *Appl. Phys. Lett.* **2005**, *86*, 251104.
(28) Nagase, T.; Ooie, T.; Kominami, H.; Nakanishi, Y.; Mizutani, N. *Jpn. J. Appl. Phys., Part 1* **2003**, *42*, 1179−1184.
(29) Lin, C. C.; Chen, H. P.; Liao, H. C.; Chen, S. Y. *Appl. Phys. Lett.* **2005**, *86*, 183103.
(30) Yao, B. D.; Chan, Y. F.; Wang, N. *Appl. Phys. Lett.* **2002**, *81*, 757−759.
(31) Liu, X.; Phang, J. C. H.; Chan, D. S. H.; Chim, W. K. *J. Phys. D: Appl. Phys.* **1999**, *32*, 1563−1569.
(32) Tatsumi, T.; Fujita, M.; Kawamoto, N.; Sasajima, M.; Horikoshi, Y. *Jpn. J. Appl. Phys., Part 1* **2004**, *43*, 2602−2606.
(33) Garces, N. Y.; Wang, L.; Bai, L.; Giles, N. C.; Halliburton, L. E.; Cantwell, G. *Appl. Phys. Lett.* **2002**, *81*, 622−624.

NL071959O